Cavity-induced modifications to the resonance fluorescence and probe absorption of a laser-dressed V-type atom

Jin-Sheng Peng,[1,2] Gao-Xiang Li,[1] Peng Zhou,[2] and S. Swain[2]
[1]*Department of Physics, Huazhong Normal University, Wuhan 430079, China*
[2]*Department of Applied Mathematics and Theoretical Physics, The Queen's University of Belfast, Belfast BT7 1NN, United Kingdom*
(Received 17 September 1999; revised manuscript received 25 January 2000; published 11 May 2000)

A cavity-modified master equation is derived for a coherently driven, V-type three-level atom coupled to a single-mode cavity in the bad-cavity limit. We show that population inversion in both the bare- and dressed-state bases may be achieved, originating from the enhancement of the atom-cavity interaction when the cavity is resonant with an atomic dressed-state transition. The atomic populations in the dressed-state representation are analyzed in terms of the cavity-modified transition rates. The atomic fluorescence spectrum and probe absorption spectrum are also investigated, and it is found that the spectral profiles may be controlled by adjusting the cavity frequency. Peak suppression and line narrowing occur under the appropriate conditions.

PACS number(s): 42.50.Gy, 32.70.Jz, 42.50.Ct, 03.65.−w

I. INTRODUCTION

A major interest of modern quantum optics is to devise ways to modify and control the radiative properties of atoms. This may be achieved by changing the environment so that the atoms interact with a modified set of vacuum modes. One such modified vacuum is provided by the cavity environment [1], where the electromagnetic modes are concentrated around the cavity-resonant frequency. The coupling of the atoms to the modified electromagnetic vacuum is therefore frequency dependent. For an excited atom located inside such a cavity, the cavity mode is the only one available to the atom for emission. If the atomic transition is in resonance with the cavity, the spontaneous emission rate into the particular cavity mode is enhanced [2]; otherwise, it is inhibited [3]. When the atom is strongly driven by a laser field, the atom-laser system may be considered to form a new dressed atom [4,5] whose energy-level structure is intensity dependent. For such a coherently driven two-level atom placed inside a cavity, theoretical investigations have predicted a phenomenological richness that is not found in the absence of the strong driving field—for example, dynamical suppression of the spontaneous emission rate [6,7], population inversion in both bare- and dressed-state bases [7,8], and distortion and narrowing of the Mollow triplet [7,9]. All these features are very sensitive to the cavity resonance frequency because of the cavity enhancement of the dressed atomic transitions.

Recently, Lange and Walther [10] have observed the dynamical suppression of spontaneous emission in a microwave cavity. In the optical-frequency regime, Zhu *et al.* [11] have also reported experimental studies of the effects of cavity detuning on the radiative properties of a coherently driven two-level atom. They have shown that the atomic fluorescence of a strongly driven two-level atom is enhanced when the cavity frequency is tuned to one of the sidebands of the Mollow fluorescence triplet, whereas it is inhibited by tuning to the other sideband. The enhancement of atomic resonance fluorescence at one sideband is a direct demonstration of population inversion.

In this paper, we investigate the dynamical modification of the resonance fluorescence of a coherently driven V-type three-level atom coupled to a frequency-tunable, single-mode cavity in the bad-cavity limit. We demonstrate that the atomic populations, fluorescence spectrum, and absorption spectrum can be strongly controlled and manipulated by tuning the cavity frequency. In Sec. II, we derive a cavity-modified master equation for the atomic density-matrix operator from the full master equation by adiabatically eliminating the cavity variables in the bad-cavity limit. For simplicity, we restrict attention to the situation where the laser frequency is tuned to the mean Bohr frequency of the excited states. The results obtained here are basic to the whole paper, and the equations derived in this section are used to calculate *all* the numerical results presented. The first part of Sec. III is devoted to discussing the atomic population distribution in the bare-state representation. It is pointed out that significant population inversions can be achieved. In the second part of Sec. III, we analyze the equations for the populations in the dressed-state basis, with particular emphasis on the high-field limit. We find that the dressed-state populations obey rate equations, with atomic transition rates that are strongly dependent on the Rabi frequency and the cavity resonance frequency. Under certain conditions, the population may also be inverted in the dressed-state basis. The plots of the dressed-state populations against the cavity-frequency–laser-frequency detuning are used to provide a semiquantitative understanding of the phenomena described in the subsequent sections. In Sec. IV, we study the cavity effects on the resonance fluorescence spectra of this system. It is shown that dynamical control of the populations and fluorescence spectrum by adjustment of the cavity resonance frequency and Rabi frequency is possible. Peak-suppression and line-narrowing phenomena are also revealed. In Sec. V, we briefly consider the absorption of a weak tunable probe field transmitted through this system, and in Sec. VI we give a summary.

II. THE CAVITY-MODIFIED MASTER EQUATION

Consider a V-configuration atom consisting of two excited states $|1\rangle$ and $|2\rangle$ coupled to a ground state $|0\rangle$ by a

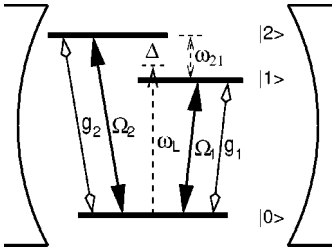

FIG. 1. Configuration of a V-type three-level atom coupled to a single-mode cavity and driven by a laser field.

single-mode cavity field of frequency ω_C and a laser field with frequency ω_L, as shown in Fig. 1. The cavity mode is described by the annihilation and creation operators a and $a^\dagger$, while the atom is represented by the operators $A_{lk} \equiv |l\rangle\langle k|$ $(l,k=0,1,2)$. In the frame rotating at the frequency ω_L, and within the rotating wave approximation, the master equation for the density-matrix operator ρ of the combined atom-cavity system is

$$\dot{\rho}_T = -i[H_A + H_C + H_I, \rho_T] + \mathcal{L}_A\rho_T + \mathcal{L}_C\rho_T, \tag{1}$$

where

$$H_A = (\Delta - \omega_{21})A_{11} + \Delta A_{22} + \Omega_2(A_{02} + A_{20}) + \Omega_1(A_{01} + A_{10}), \tag{2a}$$

$$H_C = \delta a^\dagger a, \tag{2b}$$

$$H_I = g_2(a^\dagger A_{02} + A_{20}a) + g_1(a^\dagger A_{01} + A_{10}a), \tag{2c}$$

$$\mathcal{L}_A\rho_T = \frac{\gamma_1}{2}(2A_{01}\rho_T A_{10} - \rho_T A_{11} - A_{11}\rho_T) + \frac{\gamma_2}{2}(2A_{02}\rho_T A_{20} - \rho_T A_{22} - A_{22}\rho_T), \tag{2d}$$

$$\mathcal{L}_C\rho_T = \kappa(2a\rho_T a^\dagger - a^\dagger a\rho_T - \rho_T a^\dagger a), \tag{2e}$$

with

$$\omega_{21} = \omega_2 - \omega_1, \quad \delta = \omega_C - \omega_L, \quad \text{and} \quad \Delta = \omega_2 - \omega_L. \tag{3}$$

Here H_A and H_C describe the coherently driven atom and the cavity, respectively, and H_I represents the interaction between the atom and the cavity mode. The Rabi frequency Ω_j relates to the atomic transitions $|j\rangle \leftrightarrow |0\rangle$ $(j=1,2)$ under the action of the driving laser field, and g_j is the coupling constant between the atom and the cavity mode associated with the same transition. $\mathcal{L}_C\rho_T$ and $\mathcal{L}_A\rho_T$ describe, respectively, the damping of the cavity field by a standard vacuum reservoir, and the atomic damping to background modes other than the privileged cavity modes. γ_1 and γ_2 are just the spontaneous decay constants of the levels $|1\rangle$ and $|2\rangle$. Here we also assume that the atomic-dipole moments $\mathbf{d}_{10}$ and $\mathbf{d}_{20}$ are orthogonal to each other, so that there is no spontaneously generated quantum interference [12] resulting from the cross coupling between the transitions $|1\rangle \leftrightarrow |0\rangle$ and $|2\rangle \leftrightarrow |0\rangle$. For simplicity in the resulting expressions, we assume $\Omega_1 = \Omega_2 = \Omega$, $g_1 = g_2 = g$, $\gamma_1 = \gamma_2 = \gamma$, and $\Delta = \omega_{21}/2$ in what follows.

We assume that the atom-cavity coupling is weak and the cavity has a low-Q value, so that

$$\kappa \gg g \gg \gamma \tag{4}$$

(the bad-cavity limit). This condition implies that the cavity-mode response to the standard vacuum reservoir is much faster than that produced by its interaction with the atom. Then the atom always experiences the cavity mode in the state induced by the vacuum reservoir, and this permits one to eliminate the variables containing the cavity-field operators adiabatically, giving rise to a reduced master equation for the atomic variables only. As the derivation is tedious, we refer readers to [7,10], and here outline only the key points.

We temporarily disregard $\mathcal{L}_A\rho_T$ in the elimination of the cavity mode, since it is unchanged by these operations. First, we perform a canonical transformation to the atom-cavity interaction picture [Eq. (1)] by

$$\tilde{\rho}_T = e^{i(H_A + H_C)t}\rho_T e^{-i(H_A + H_C)t}. \tag{5}$$

The master equation then takes the form

$$\partial_t(e^{-\mathcal{L}_C t}\tilde{\rho}_T) = -ie^{-\mathcal{L}_C t}[\tilde{H}_I(t), \tilde{\rho}_T], \tag{6}$$

where $\tilde{H}_I(t) = g[\tilde{D}(t)a^\dagger \exp(i\delta t) + \text{H.c.}]$, with $\tilde{D}(t) = \exp(iH_A t)D\exp(-iH_A t)$ and $D = A_{01} + A_{02}$. We next introduce the operator χ:

$$\chi = e^{-\mathcal{L}_C t}\tilde{\rho}_T, \tag{7}$$

which, according to Eq. (6), obeys the equation

$$\dot{\chi}(t) = -ige^{\kappa t}\{[a^\dagger, \tilde{D}(t)\chi(t)]e^{i\delta t} + [a, \chi(t)\tilde{D}^\dagger(t)]e^{-i\delta t}\} - ige^{-\kappa t}\{[\tilde{D}(t), \chi(t)a^\dagger]e^{i\delta t} + [\tilde{D}^\dagger(t), a\chi(t)]e^{-i\delta t}\}. \tag{8}$$

Due to the smallness of the coupling constant g, we can perform a second-order perturbation calculation with respect to g by means of standard projection operator techniques. Noting that

$$\text{Tr}_C\chi(t) \equiv \text{Tr}_C\tilde{\rho}_T(t) \equiv \tilde{\rho}(t), \tag{9}$$

we can trace out the cavity variables to obtain the master equation for the reduced-density matrix operator $\tilde{\rho}$ of the atom. Under the Born-Markovian approximation, the resulting master equation is of the form

$$\tilde{\rho}(t) = -g^2\int_0^\infty \{e^{-(\kappa + i\delta)\tau}[\tilde{D}^\dagger(t)\tilde{D}(t-\tau)\tilde{\rho}(t) - \tilde{D}(t-\tau)\tilde{\rho}(t)\tilde{D}^\dagger(t)] + \text{H.c.}\}d\tau.$$

Finally, transforming $\tilde{\rho}$ back to the original picture via $\rho = \exp(-iH_A t)\tilde{\rho}\exp(iH_A t)$, and restoring the $\mathcal{L}_A\rho$ contribution, we express the reduced master equation for the atomic variables as

$$\dot{\rho} = -i[H_A,\rho] + \frac{\gamma_c}{2}(D\rho S^\dagger + S\rho D^\dagger - D^\dagger S\rho - \rho S^\dagger D) + \frac{\gamma}{2}(2A_{01}\rho A_{10} - \rho A_{11} - A_{11}\rho) + \frac{\gamma}{2}(2A_{02}\rho A_{20} - \rho A_{22} - A_{22}\rho), \tag{10}$$

where $\gamma_c = 2g^2/\kappa$ specifies the emission rate of the atom into the cavity mode, and

$$S = \kappa\int_0^\infty e^{-(\kappa+i\delta)\tau}\tilde{D}(-\tau)d\tau = \beta_0 A_{00} + \beta_1 A_{11} + \beta_2 A_{22} + \beta_3 A_{10} + \beta_4 A_{01} + \beta_5 A_{20} + \beta_6 A_{02} + \beta_7 A_{21} + \beta_8 A_{12}, \tag{11}$$

where the coefficients β_i $(i=0,1,\ldots,8)$ are given by

$$\begin{bmatrix}\beta_0\\ \beta_1\\ \beta_2\\ \beta_3\\ \beta_4\\ \beta_5\\ \beta_6\\ \beta_7\\ \beta_8\end{bmatrix} = \begin{bmatrix} 0 & 2\eta\varepsilon^2 & -2\eta\varepsilon^2 & 8\eta^3 & -8\eta^3\\ -2\eta\varepsilon & \eta\varepsilon(1-\varepsilon) & \eta\varepsilon(1+\varepsilon) & -\eta(1-\varepsilon^2)/2 & \eta(1-\varepsilon^2)/2\\ 2\eta\varepsilon & -\eta\varepsilon(1+\varepsilon) & -\eta\varepsilon(1-\varepsilon) & -\eta(1-\varepsilon^2)/2 & \eta(1-\varepsilon^2)/2\\ 4\eta^2 & 4\eta^2\varepsilon & -4\eta^2\varepsilon & -2\eta^2(1+\varepsilon) & -2\eta^2(1-\varepsilon)\\ 4\eta^2 & \varepsilon^2(1-\varepsilon)/2 & \varepsilon^2(1+\varepsilon)/2 & 2\eta^2(1-\varepsilon) & 2\eta^2(1+\varepsilon)\\ 4\eta^2 & -4\eta^2\varepsilon & 4\eta^2\varepsilon & -2\eta^2(1-\varepsilon) & -2\eta^2(1+\varepsilon)\\ 4\eta^2 & \varepsilon(1+\varepsilon)/2 & \varepsilon(1-\varepsilon)/2 & 2\eta^2(1+\varepsilon) & 2\eta^2(1-\varepsilon)\\ 0 & -\eta\varepsilon(1-\varepsilon) & -\eta\varepsilon(1+\varepsilon) & -\eta(1-\varepsilon)^2/2 & \eta(1+\varepsilon)^2/2\\ 0 & \eta\varepsilon(1+\varepsilon) & \eta\varepsilon(1-\varepsilon) & -\eta(1+\varepsilon)^2/2 & \eta(1-\varepsilon)^2/2\end{bmatrix}\begin{bmatrix}\frac{\kappa}{\kappa+i\delta}\\ \frac{\kappa}{\kappa+i(\delta-\Omega_R)}\\ \frac{\kappa}{\kappa+i(\delta+\Omega_R)}\\ \frac{\kappa}{\kappa+i(\delta-2\Omega_R)}\\ \frac{\kappa}{\kappa+i(\delta+2\Omega_R)}\end{bmatrix}, \tag{12}$$

with

$$\Omega_R = \frac{1}{2}\sqrt{\omega_{21}^2+8\Omega^2}, \quad \eta = \frac{\Omega}{2\Omega_R}, \quad \varepsilon = \frac{\omega_{21}}{2\Omega_R}. \tag{13}$$

The first term of Eq. (10) describes the coherent evolution of the atom, the second term the cavity-induced decay of the atom into the cavity mode, and the remaining terms the spontaneous atomic emissions to the background modes.

The equations of motion for the atomic variables take the form

$$\dot{\rho}_{11} = -\gamma\rho_{11} - i\Omega(\rho_{01}-\rho_{10}) - \frac{\gamma_c}{2}(\beta_0\rho_{01} + \beta_0^*\rho_{10} + \beta_4\rho_{11} + \beta_4^*\rho_{11} + \beta_6\rho_{21} + \beta_6^*\rho_{12}), \tag{14}$$

$$\dot{\rho}_{22} = -\gamma\rho_{22} - i\Omega(\rho_{02}-\rho_{20}) - \frac{\gamma_c}{2}(\beta_0\rho_{02} + \beta_0^*\rho_{20} + \beta_4\rho_{12} + \beta_4^*\rho_{21} + \beta_6\rho_{22} + \beta_6^*\rho_{22}),$$

$$\dot{\rho}_{10} = -\frac{1}{2}(\gamma - i\omega_{21})\rho_{10} + i\Omega(\rho_{11}-\rho_{00}+\rho_{12}) - \frac{\gamma_c}{2}[\beta_0\rho_{00} - \beta_1(\rho_{11}+\rho_{12}) - \beta_3(\rho_{01}+\rho_{02}) + \beta_4\rho_{10} + \beta_6\rho_{20} - \beta_8(\rho_{21}+\rho_{22})],$$

$$\dot{\rho}_{20} = -\frac{1}{2}(\gamma + i\omega_{21})\rho_{20} + i\Omega(\rho_{22}-\rho_{00}+\rho_{21}) - \frac{\gamma_c}{2}[\beta_0\rho_{00} - \beta_2(\rho_{21}+\rho_{22}) - \beta_5(\rho_{01}+\rho_{02}) + \beta_4\rho_{10} + \beta_6\rho_{20} - \beta_7(\rho_{11}+\rho_{12})],$$

$$\dot{\rho}_{21} = -(\gamma + i\omega_{21})\rho_{21} - i\Omega(\rho_{01}-\rho_{20}) - \frac{\gamma_c}{2}(\beta_0\rho_{01} + \beta_0^*\rho_{20} + \beta_4\rho_{11} + \beta_4^*\rho_{21} + \beta_6\rho_{21} + \beta_6^*\rho_{22}),$$

III. STEADY-STATE POPULATIONS

A. The bare states

We have numerically solved Eq. (14) for the populations in the steady state. In all our numerical plots, we assume the

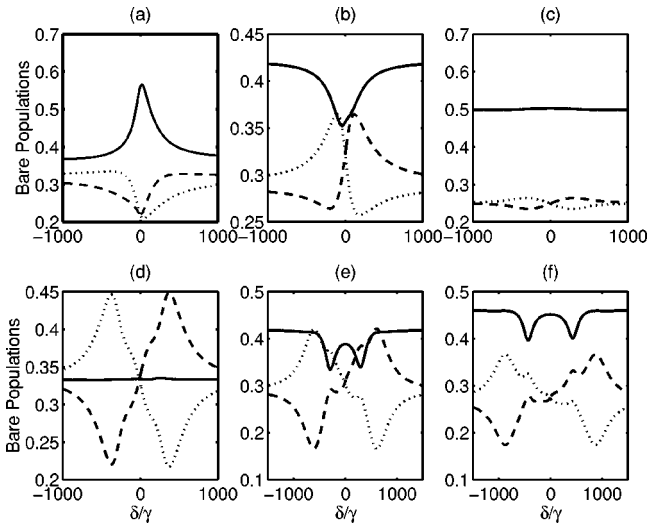

FIG. 2. The bare-state populations of a V-type three-level atom coupled to a single-mode cavity and driven by a laser field. The ground-state population is represented by a solid line, the first excited state by a dashed line, and the second excited state by a dotted line. In all our figures, we assume the values $\gamma=1$, $g=20$, $\kappa=100$. In the first three frames here, we assume $\omega_{21}=10$, and in the last three $\omega_{21}=100$. In frames (a), (b), and (c), we take $\Omega=4$, 10, and 100, respectively, and in frames (d), (e), and (f) we take $\Omega=100$, 200, and 300, respectively.

values $\gamma=1$, $g=20$, and $\kappa=100$, so that the condition of Eq. (4) is satisfied. All the frequencies are also measured in units of γ.

In Fig. 2, we plot the bare-state populations as a function of the cavity-laser detuning δ. We first consider the case where $\omega_{21}=10$, taking in frame (a), $\Omega=4$; in frame (b), $\Omega=10$; and in frame (c), $\Omega=100$. For the smallest value of Ω, all three populations tend to have roughly the same value for large detunings, but for small detunings, a resonant effect is evident around $\delta=0$: the population in the ground state passes through a maximum, while the population in the two excited states exhibits a minimum. The behavior in frame (b) is qualitatively different; here, the population resides mainly in the ground state, but this population now shows a dip as δ passes through zero. The excited-state populations show a minimum and a maximum close to the origin. There is a very tiny amount of population inversion for state $|2\rangle$ over state $|0\rangle$ for a very short range of negative detunings close to zero, but the effect is unimportant. As the value of Ω is increased to $\Omega=100$ in frame (c), keeping $\omega_{21}=10$, the populations show a flatter behavior, with the ground-state population tending to the value 0.5 for large δ, and that of the excited states to the value 0.25. The minimum in the ground-state population at $\delta=0$ in frame (b) has been replaced by a very shallow maximum in frame (c). It is clear that the most interesting behavior arises for $\Omega\sim\omega_{21}$.

In the next three frames we assume a larger value for the excited-state splitting, $\omega_{21}=200$. For the lowest value of Ω considered, $\Omega=100$, the behavior in frame (d) is qualitatively different from that shown in the first three frames. Now all three bare populations tend toward the same value for large δ. The ground-state population is almost flat, but

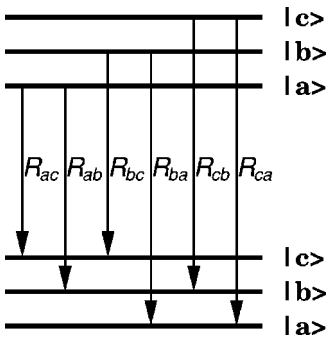

FIG. 3. Diagram of atomic dressed states and dressed-state transitions.

the excited states possess pronounced maxima and minima, as well as the suggestion of further structure. It is clear that, for appropriate detunings, a large population inversion between the excited and ground states can be achieved. When Ω is increased to $\Omega=200$, as in frame 2(e), the ground-state population begins to increase, decreasing the population inversion obtainable. Also, structure at four different frequencies becomes evident. (The reasons for this will become apparent in Sec. III B.) The trend continues in the final frame, where $\Omega=300$, and there is no population inversion. For still larger values of Ω (not shown), the ground-state population tends to flatten around the value 0.5, and the excited-state populations around the value 0.25, as in frame 2(c) but with different detailed structure.

B. The dressed states

To study the modification of the atomic populations due to the presence of the cavity, we work in the semiclassical dressed-state representation. The dressed states, defined by the eigenvalue equation, $H_A|\alpha\rangle=\lambda_\alpha|\alpha\rangle$, are of the form [12]

$$|a\rangle=\frac{1}{2}[-(1-\varepsilon)|2\rangle-(1+\varepsilon)|1\rangle+4\eta|0\rangle],$$

$$|b\rangle=-2\eta|2\rangle+2\eta|1\rangle+\varepsilon|0\rangle, \tag{15}$$

$$|c\rangle=\frac{1}{2}[(1+\varepsilon)|2\rangle+(1-\varepsilon)|1\rangle+4\eta|0\rangle],$$

and the corresponding energies are

$$\lambda_a=-\Omega_R, \quad \lambda_b=0, \quad \lambda_c=\Omega_R. \tag{16}$$

Within the secular approximation, the equations of motion for the populations in the dressed states may be cast into the rate-equation form

$$\dot{\rho}_{aa}=-(R_{ab}+R_{ac})\rho_{aa}+R_{ca}\rho_{cc}+R_{ba}\rho_{bb},$$

$$\dot{\rho}_{bb}=-(R_{bc}+R_{ba})\rho_{bb}+R_{cb}\rho_{cc}+R_{ab}\rho_{aa}, \tag{17}$$

$$\dot{\rho}_{cc}=-(R_{ca}+R_{cb})\rho_{cc}+R_{ac}\rho_{aa}+R_{bc}\rho_{bb},$$

where $R_{\alpha\beta}$ $(\alpha,\beta=a,b,c)$ represents the atomic transition rate from the substate $|\alpha\rangle$ of one dressed-state triplet to the substate $|\beta\rangle$ of the dressed-state triplet below, as depicted in Fig. 3. In the high-field limit, that is, when the effective Rabi frequency is much greater than all the relaxation rates, $\Omega_R \gg \gamma, \gamma_c$, the coupling between atomic density-matrix elements $\rho_{\alpha\beta}$ associated with the various frequencies may be omitted to $O(\gamma/\Omega_R)$ and $O(\gamma_c/\Omega_R)$, and the transition rates may be expressed as

$$
\begin{aligned}
R_{bc} &= R_{ba} = \frac{\gamma}{2}(1-\varepsilon^2)^2, \\
R_{ab} &= \frac{\gamma}{2}(1+\varepsilon^2)\varepsilon^2 + \gamma_c \varepsilon^2 \mathcal{R}(\Omega_R), \\
R_{cb} &= \frac{\gamma}{2}(1+\varepsilon^2)\varepsilon^2 + \gamma_c \varepsilon^2 \mathcal{R}(-\Omega_R), \\
R_{ac} &= \frac{\gamma}{4}(1-\varepsilon^4) + \gamma_c 4\eta^2 \mathcal{R}(2\Omega_R), \\
R_{ca} &= \frac{\gamma}{4}(1-\varepsilon^4) + \gamma_c 4\eta^2 \mathcal{R}(-2\Omega_R),
\end{aligned}
\tag{18}
$$

where $\mathcal{R}(\pm x) = \kappa^2/[\kappa^2 + (\delta \pm x)^2]$. The above expressions for the transition rates will provide the basis for the physical explanation of the effects to be described.

The function $\mathcal{R}(\pm 2\Omega_R)$ introduces resonances at $\delta = \pm 2\Omega_R$ into the rates R_{ac} and R_{ca} with a strength proportional to $4\Omega^2$. This appears to be more dominant than the resonances at $\delta = \pm \Omega_R$, which occur in R_{cb} and R_{ab} with a strength proportional to ω_{21}^2. Resonances at $\delta = \pm 2\Omega_R$ can be clearly seen in frames (b)–(f) of Fig. 2, whereas resonances at $\delta = \pm \Omega_R$ are only apparent in frames (c)–(f).

Equations (18) show that, in the presence of the cavity, the transition rates R_{ab}, R_{ac}, R_{cb}, and R_{ca} are strongly dependent on the cavity frequency, but R_{bc} and R_{ba} are only related to the spontaneous emission rate. This is because, for the system considered here, a V-type three-level atom interacting with the cavity mode, there exist nine double channels for the atomic transition from the dressed states $|i\rangle$ to $|j\rangle$, which originate from the atomic bare-state transitions $|1\rangle$ to $|0\rangle$ and $|2\rangle$ to $|0\rangle$, respectively. Constructive or destructive interference happens within every double channel. But the two double channels for the transitions $|b\rangle \rightarrow |c\rangle$ and $|b\rangle \rightarrow |a\rangle$ are completely destructive for the cavity mode—that is, the transitions from $|b\rangle$ to $|c\rangle$ and from $|b\rangle$ to $|a\rangle$ never result in the emission of a photon into the cavity mode. So the atomic transition rates R_{bc} and R_{ba} are only dependent on the spontaneous emission rate and are independent of the cavity frequency. As the other seven double channels are still open to the cavity mode, this means that for the other transitions from $|i\rangle$ to $|j\rangle$ a cavity photon can be generated, but it will be very strongly damped under the bad-cavity assumption. Therefore, besides the terms describing atomic photon emission into the background, there occur additional terms dependent on the cavity frequency in the transition rates R_{ab}, R_{ac}, R_{cb}, and R_{ca}.

The steady-state dressed populations are found from Eqs. (17) to be

$$
\begin{aligned}
\rho_{aa} &= \frac{R_{ba}(R_{ca}+R_{cb}+R_{bc}) + R_{bc}(R_{ca}-R_{ba})}{(R_{ab}+R_{ac}+R_{ba})(R_{ca}+R_{cb}+R_{bc}) - (R_{ca}-R_{ba})(R_{ac}-R_{bc})}, \\
\rho_{cc} &= \frac{R_{ba}(R_{ac}-R_{bc}) + R_{bc}(R_{ab}+R_{ac}+R_{ba})}{(R_{ab}+R_{ac}+R_{ba})(R_{ca}+R_{cb}+R_{bc}) - (R_{ca}-R_{ba})(R_{ac}-R_{bc})}, \\
\rho_{bb} &= 1 - \rho_{aa} - \rho_{cc}.
\end{aligned}
\tag{19}
$$

The dressed-state populations are plotted as a function of the detuning in Fig. 4 for the same parameter values employed in Fig. 3. These plots have been obtained by a numerical solution of Eqs. (14), but we have found that the Eqs. (19) provide an excellent approximation in the strong-field limit.

It is evident that, if the excited levels of the V atom are degenerate $(\varepsilon = 0)$ or nearly degenerate $(\varepsilon \simeq 0)$, the transitions $|a\rangle \rightarrow |b\rangle$ and $|c\rangle \rightarrow |b\rangle$ are turned off (as $R_{ab}, R_{cb} \sim \varepsilon^2$), whereas the rate of transitions out of the dressed state $|b\rangle$, $R_{ba}+R_{bc}$, is nonzero. Thus there is no steady-state population in the dressed-state $|b\rangle$, only in the dressed states $|a\rangle$ and $|c\rangle$. In general, it follows that in the regime $\Omega^2 \gg \omega_{21}^2$, the population in dressed state $|b\rangle$ is very small. Furthermore, if the cavity frequency is tuned to $\delta = -2\Omega_R$, the dressed-state transition from $|a\rangle$ to $|c\rangle$ is resonantly enhanced $(R_{ac} \simeq \gamma/4 + \gamma_c 4\eta^2)$, while the reverse transition is suppressed $(R_{ca} \simeq \gamma/4)$, and thus more population will be accumulated into the state $|c\rangle$. For $\delta = 2\Omega_R$, there exists a greater population in the dressed state $|a\rangle$. An example is shown in frame (c) of Fig. 4, where we take $\omega_{21} = 10$, $\Omega = 100$. (The population in $|b\rangle$ is very close to zero.) In frame (f), where we are only beginning to approach the limit $\Omega^2 \gg \omega_{21}^2$, the behavior is similar, but now there is a small but significant population in state $|b\rangle$.

However, in the opposite limit, where the excited-level splitting is much greater than the Rabi frequency $(\omega_{21}^2 \gg \Omega^2)$, the transition rates R_{ac}, R_{ca}, R_{ba}, and R_{bc} are very small, and the transitions into the dressed state $|b\rangle$, represented by R_{ab} and R_{cb}, dominate. Eventually, the population in the dressed state $|b\rangle$ approaches unity, and the

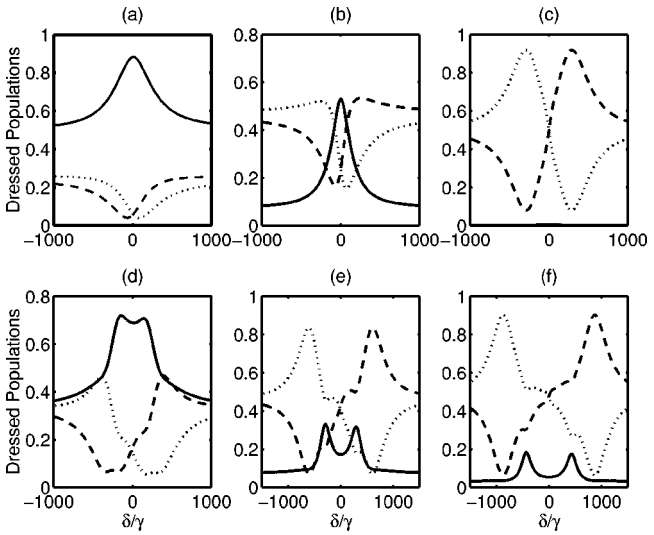

FIG. 4. The dressed-state populations, for the same parameters used in Fig. 2. The dressed state ''b'' is represented by a solid line, the dressed state ''a'' by a dashed line, and the dressed state ''c'' by a dotted line. In the first three frames, $\omega_{21}=10$, and in the last three $\omega_{21}=100$. In frames (a), (b), and (c), $\Omega=4$, 10, and 100, respectively, and in frames (d), (e), and (f), $\Omega=100$, 200, and 300, respectively.

population in the states $|a\rangle$ and $|c\rangle$ is very small. In this case, the resonance features of the dressed-state populations regarding the cavity frequency are less pronounced. We do not plot this case here, but the features can be seen beginning to emerge in frame (a), and to a lesser extent in frame (c). The intermediate regime, where $\omega_{21}=\Omega$, is shown in frames (b) and (e).

In general, the population distributions are strongly dependent on the cavity frequency. For example, when $\delta=0$ the cavity is tuned to resonance with the driving field, and we have $R_{ab}=R_{cb}$, $R_{ba}=R_{bc}$, and $R_{ac}=R_{ca}$. Consequently, there is no population difference between the upper dressed state $|c\rangle$ and the lower one $|a\rangle$. Moreover, in the case $\Omega_R \gg \kappa$, the distribution is the same as in free space [12].

When the cavity frequency satisfies $\delta=-\Omega_R$, describing resonance with the dressed-state transition $|a\rangle \rightarrow |b\rangle$, the rate of this transition R_{ab} is greatly enhanced. Also, the rate of downward atomic transitions from $|a\rangle$ to $|c\rangle$ is larger than the transition rate $|c\rangle \rightarrow |a\rangle$, i.e., $R_{ac}>R_{ca}$. As a result, the population in the dressed state $|c\rangle$ is greater than that in the state $|a\rangle$ ($\rho_{cc}>\rho_{aa}$).

A similar analysis shows that the population ρ_{cc} of the state $|c\rangle$ is also greater than the population ρ_{aa} of the dressed state $|a\rangle$ if the cavity is tuned to $\delta=-2\Omega_R$. The opposite conclusions hold when $\delta=\Omega_R$ and $2\Omega_R$, as is clearly demonstrated in Figs. 4(c)–4(f) for different values of the Rabi frequency Ω.

If the cavity is tuned to resonance with the driving field ($\delta=0$), then $R_{ab}=R_{cb}$, $R_{ca}=R_{ac}$, and $R_{bc}=R_{ba}$. From Fig. 2 we see that the population distribution between the dressed states $|c\rangle$ and $|a\rangle$ is balanced, which is similar to the case in the absence of the cavity [12]. In the presence of the cavity, the transition rates R_{ab} and R_{cb} from the dressed states $|a\rangle$ and $|c\rangle$ to the dressed state $|b\rangle$ are faster than those in the absence of the cavity, while the reverse rates R_{bc} and R_{ba} remain unchanged because of the closing of the atomic transitions $|b\rangle \rightarrow |c\rangle$ and $|b\rangle \rightarrow |a\rangle$ for the cavity mode caused by destructive interference. The populations ρ_{cc} and ρ_{aa} are decreased and ρ_{bb} is increased by comparison with the case in the absence of the cavity.

However, when the cavity frequency is tuned to satisfy $\delta=-\Omega_R$, the atomic transition from $|a\rangle$ to $|b\rangle$, which occurs at frequency $\omega_L-\Omega_R$, is resonant with the cavity. The interaction of the atom with the privileged cavity mode is enhanced, and the atom predominately (since $g \gg \gamma$) emits a photon into the cavity mode, characterized by the $\varepsilon^2\gamma_c$ term in R_{ab}, in addition to radiating a photon into the background, represented by the term Γ_0 in R_{ab}. In contrast, the other transitions describing atomic emission of a photon into the cavity mode are far off resonance with the cavity (since $\Omega_R \gg \kappa$), so the atom can only radiate a photon into the background. As a consequence, the symmetry of the transitions from $|c\rangle$ to $|b\rangle$ and from $|a\rangle$ to $|b\rangle$ is broken, which results in an enhanced population in the dressed state $|c\rangle$ over that in $|a\rangle$.

When the cavity frequency is tuned to satisfy $\delta=-2\Omega_R$, the atomic transition rate R_{ac} at the cavity frequency $\omega_L-2\Omega_R$ is resonantly enhanced, and the other three rates R_{ab}, R_{cb}, and R_{ca} are decreased. In this case, if $\gamma_c \gg \gamma(1+\varepsilon^2)/(1-\varepsilon^2)$, the other five transition rates are much smaller than R_{ca}. Thus any population in the dressed state $|a\rangle$, resulting from transitions from $|b\rangle$ and $|c\rangle$ to $|a\rangle$, will return to $|c\rangle$ very quickly because R_{ac} is much greater than the other transition rates. So it seems that the atom is trapped in the two dressed states $|b\rangle$ and $|c\rangle$, and the population in the state $|a\rangle$ approaches zero. Similar explanations can be adopted for the cases $\delta=\Omega_R$ and $\delta=2\Omega_R$.

IV. RESONANCE FLUORESCENCE SPECTRUM

The spectrum of the atomic fluorescence emission emitted from the side of the cavity is proportional to the Fourier transform of the steady-state correlation function $\lim_{t\rightarrow\infty}\langle \vec{E}^{(-)}(\vec{r},t+\tau)\cdot\vec{E}^{(+)}(\vec{r},t)\rangle$, where $\vec{E}^{(\pm)}(\vec{r},t)$ are the positive and negative frequency parts of the radiation field in the far zone, which consists of a free-field operator and a source field that is proportional to the atomic polarization operator. The fluorescence spectrum is given by

$$\Lambda(\omega)=\mathrm{Re}\int_0^\infty [\langle A_{20}(t+\tau),A_{02}(t)\rangle + \langle A_{10}(t+\tau),A_{01}(t)\rangle]_{t\rightarrow\infty}e^{-i\omega\tau}d\tau. \quad (20)$$

Because we have assumed that the atomic dipole moment elements $\vec{d}_{20}$ and $\vec{d}_{10}$ are perpendicular to each other, the two correlation functions $\langle A_{10}(t+\tau),A_{02}(t)\rangle$ and $\langle A_{20}(t+\tau),A_{01}(t)\rangle$ make no contribution to the fluorescence emission spectrum. Using the quantum regression theorem, the spectrum may be expressed as

$$\Lambda(\omega)=\mathrm{Re}\{\tilde{F}_{01}(z)+\tilde{G}_{02}(z) -[|\rho_{01}(\infty)|^2+|\rho_{02}(\infty)|^2]/z\}_{z=i\omega}, \quad (21)$$

where $\tilde{X}(z)$ denotes the Laplace transform of $X(\tau)$, and

$$F(\tau)=U^{\dagger}(\tau)[|0\rangle\langle 1|\rho(\infty)]U(\tau)$$

and

$$G(\tau)=U^{\dagger}(\tau)[|0\rangle\langle 2|\rho(\infty)]U(\tau), \quad (22)$$

with $U(t)$ the time development operator, obey the same equation of motion as $\rho(\tau)$ but with the different initial conditions implied by the definitions (22).

We calculate the resonance fluorescence spectra numerically from the equations obtained in Sec. II. However, the dressed-atom approach provides a convenient way of interpreting the results so obtained, at least in the strong-field limit, and so we develop this approach here. In terms of the dressed states (15), we have, for example,

$$\tilde{F}_{01}(z)=\sum_{\alpha,\beta=a,b,c}\langle 0|\alpha\rangle\tilde{F}_{\alpha\beta}(z)\langle\beta|1\rangle, \quad (23)$$

with the initial condition

$$F_{\alpha\beta}(0)=\sum_{\gamma}\langle\alpha|0\rangle\rho_{\gamma\beta}(\infty)\langle 1|\beta\rangle. \quad (24)$$

In the high-field limit, $\Omega_R\gg\gamma,\gamma_c$, which is the condition for the secular approximation to hold, the dressed energy levels are well separated, and one can associate the diagonal terms on the right-hand side of Eq. (23) and those in the corresponding equation for $\tilde{G}_{02}(z)$ with the resonance fluorescence line at the center of the spectrum, $\omega=\omega_L$ (see Fig. 3). In a similar way, the elements $\tilde{F}_{ab}$, $\tilde{G}_{ab}$, $\tilde{F}_{bc}$, and $\tilde{G}_{bc}$ are associated with the line at $\omega=\omega_L-\Omega_R$, while the elements $\tilde{F}_{ba}$, $\tilde{G}_{ba}$, $\tilde{F}_{cbc}$, and $\tilde{G}_{cb}$ are associated with the line at $\omega=\omega_L+\Omega_R$. Finally, $\tilde{F}_{ac}$ and $\tilde{G}_{ac}$ are associated with the line at $\omega=\omega_L+2\Omega_R$, and $\tilde{F}_{ca}$ and $\tilde{G}_{ca}$ with the line at $\omega=\omega_L-2\Omega_R$

One can apply the secular approximation to simplify the equations of motion for the atomic density-matrix elements in the dressed-state representation, which are obtained as follows according to Eq. (10):

$$\begin{aligned}
\dot{\rho}_{aa}&=-\Gamma_{1a}\rho_{aa}+\Gamma_{2a}\rho_{cc}+R_{ba},\\
\dot{\rho}_{cc}&=-\Gamma_{1b}\rho_{cc}+\Gamma_{2b}\rho_{aa}+R_{bc},\\
\dot{\rho}_{ab}&=-(\Gamma_{3a}-i\Omega_3)\rho_{ab}+\Gamma_4\rho_{bc},\\
\dot{\rho}_{bc}&=-(\Gamma_{3b}-i\Omega_4)\rho_{bc}+\Gamma_4\rho_{ab},\\
\dot{\rho}_{ac}&=-(\Gamma_5-i\Omega_5)\rho_{ac},
\end{aligned} \quad (25)$$

with

$$\begin{aligned}
\Gamma_{1a}&=\frac{\gamma}{4}(3-2\varepsilon^2+3\varepsilon^4)+\gamma_c[\varepsilon^2\mathcal{R}(\Omega_R)+4\eta^2\mathcal{R}(2\Omega_R)],\\
\Gamma_{1b}&=\frac{\gamma}{4}(3-2\varepsilon^2+3\varepsilon^4)+\gamma_c[\varepsilon^2\mathcal{R}(-\Omega_R)+4\eta^2\mathcal{R}(-2\Omega_R)],\\
\Gamma_{2a}&=\frac{\gamma}{2}(1-\varepsilon^2)(3\varepsilon^2-1)+\gamma_c 4\eta^2\mathcal{R}(-2\Omega_R),\\
\Gamma_{2b}&=\frac{\gamma}{2}(1-\varepsilon^2)(3\varepsilon^2-1)+\gamma_c 4\eta^2\mathcal{R}(2\Omega_R),\\
\Gamma_{3a}&=\frac{\gamma}{4}(3+\varepsilon^2-2\varepsilon^4)+\frac{\gamma_c}{2}[4\eta^2\mathcal{R}(0)+\varepsilon^2\mathcal{R}(\Omega_R)+4\eta^2\mathcal{R}(2\Omega_R)],\\
\Gamma_{3b}&=\frac{\gamma}{4}(3+\varepsilon^2-2\varepsilon^4)+\frac{\gamma_c}{2}[4\eta^2\mathcal{R}(0)+\varepsilon^2\mathcal{R}(-\Omega_R)+4\eta^2\mathcal{R}(-2\Omega_R)],\\
\Gamma_4&=-\frac{\gamma}{2}\varepsilon^2(1-\varepsilon^2),\\
\Gamma_5&=\frac{\gamma}{4}(3+\varepsilon^4)+\frac{\gamma_c}{2}\{16\eta^2\mathcal{R}(0)+\varepsilon^2[\mathcal{R}(\Omega_R)+\mathcal{R}(-\Omega_R)]+4\eta^2[\mathcal{R}(2\Omega_R)+4\eta^2\mathcal{R}(-2\Omega_R)]\},\\
\Omega_3&=\Omega_R+\frac{\gamma_c}{2}[4\eta^2\mathcal{I}(0)+\varepsilon^2\mathcal{I}(\Omega_R)+4\eta^2\mathcal{I}(2\Omega_R)],\\
\Omega_4&=\Omega_R+\frac{\gamma_c}{2}[4\eta^2\mathcal{I}(0)+\varepsilon^2\mathcal{I}(-\Omega_R)+4\eta^2\mathcal{I}(-2\Omega_R)],\\
\Omega_5&=2\Omega_R+\frac{\gamma_c}{2}\{\varepsilon^2[\mathcal{I}(\Omega_R)-\mathcal{I}(-\Omega_R)]+4\eta^2[\mathcal{I}(2\Omega_R)-\mathcal{I}(-2\Omega_R)]\},
\end{aligned} \quad (26)$$

where $\mathcal{I}(\pm x)=\kappa(\delta\pm x)/[\kappa^2+(\delta\pm x)^2]$, Γ_i is the decay rate in the dressed-state representation, which is dependent on the cavity frequency, while $\Omega_R-\Omega_{3,4}$ and $2\Omega_R-\Omega_5$ are the cavity-induced level shifts. In the bad-cavity and high-field limits, the shifts are negligibly small.

In the dressed-state representation, the underlying physical processes are very transparent. As argued in the paragraph following Eq. (23), the downward transitions between the same dressed states of two adjacent dressed-state triplets give rise to the central component of the fluorescence spectrum, i.e.,

$$\Lambda_0(\omega)=\mathrm{Re}\left[\frac{N_0(z)}{(z+\Gamma_{1a})(z+\Gamma_{1b})-\Gamma_{2a}\Gamma_{2b}}\right]_{z=i\omega}, \quad (27)$$

with

$$N_0(z)=4\eta^2(2z+\Gamma_{1a}+\Gamma_{1b}-\Gamma_{2a}-\Gamma_{2b})\rho_{aa}\rho_{cc} -2\eta^2(1-9\varepsilon^2)[\Gamma_{2a}\rho_{cc}+\Gamma_{2b}\rho_{aa}]\rho_{bb} +2\eta^2(1+9\varepsilon^2)[(z+\Gamma_{1a})\rho_{cc}+(z+\Gamma_{1b})\rho_{aa}]\rho_{bb}. \tag{28}$$

This spectral component consists of two Lorentzians with linewidths $2\gamma_0^{\pm}=(\Gamma_{1a}+\Gamma_{1b})\pm\sqrt{(\Gamma_{1a}-\Gamma_{1b})^2+4\Gamma_{2a}\Gamma_{2b}}$.

However, the downward transitions $|a\rangle\rightarrow|b\rangle$ and $|b\rangle\rightarrow|c\rangle$ from one dressed-state triplet to the next triplet lead to the lower-frequency inner sideband, yielding an expression of the form

$$\Lambda_1(\omega)=\mathrm{Re}\left[\frac{4\eta^2[8\eta^2(z+\Gamma_{3a}+i\Omega_3)-\varepsilon^2\Gamma_4]\rho_{bb}+\frac{1}{2}\varepsilon^2[(1+\varepsilon^2)(z+\Gamma_{3b}+i\Omega_4)-8\eta^2\Gamma_4]\rho_{aa}}{(z+\Gamma_{3a}+i\Omega_3)(z+\Gamma_{3b}+i\Omega_4)-\Gamma_4^2}\right]_{z=i\omega}, \tag{29}$$

while the transitions $|b\rangle\rightarrow|a\rangle$ and $|c\rangle\rightarrow|b\rangle$ between two near-lying dressed-state triplets result in the higher-frequency inner sideband,

$$\Lambda_2(\omega)=\mathrm{Re}\left[\frac{4\eta^2[8\eta^2(z+\Gamma_{3b}-i\Omega_4)-\varepsilon^2\Gamma_4]\rho_{bb}+\frac{1}{2}\varepsilon^2[(1+\varepsilon^2)(z+\Gamma_{3a}-i\Omega_3)-8\eta^2\Gamma_4]\rho_{cc}}{(z+\Gamma_{3a}-i\Omega_3)(z+\Gamma_{3b}-i\Omega_4)-\Gamma_4^2}\right]_{z=i\omega}. \tag{30}$$

Since the cavity-induced level shifts are negligible, Λ_1 will display a single spectral line located at frequency $\omega_L-\Omega_R$, and Λ_2 a line at $\omega_L+\Omega_R$. It is evident that the inner sidebands are also composed of two Lorentzians with linewidths $2\gamma_1^{\pm}=(\Gamma_{3a}+\Gamma_{3b})\pm\sqrt{(\Gamma_{3a}-\Gamma_{3b})^2+4\Gamma_4^2}$.

The final transitions, $|a\rangle\rightarrow|c\rangle$ and $|a\rangle\rightarrow|c\rangle$, respectively, generate the lower-frequency and higher-frequency spectral lines of the outer sidebands, which are given by

$$\Lambda_3(\omega)=\mathrm{Re}\left[\frac{2\eta^2(1+\varepsilon^2)\rho_{aa}}{(z+\Gamma_5+i\Omega_5)}\right]_{z=i\omega}, \tag{31}$$

$$\Lambda_4(\omega)=\mathrm{Re}\left[\frac{2\eta^2(1+\varepsilon^2)\rho_{cc}}{(z+\Gamma_5-i\Omega_5)}\right]_{z=i\omega}. \tag{32}$$

The spectral lines are centered at frequencies $\omega_L\pm2\Omega_R$, respectively, and have width $2\Gamma_5$. In Eqs. (27)–(32), the ρ_{jj} that appear are the steady-state dressed-state occupation probabilities, given by equations (19).

We first consider the fluorescence spectrum of the atom with two degenerate (or near-degenerate) excited states, where the population of the dressed state $|b\rangle$ is negligible, as illustrated in Fig. 5, where $\omega_{21}=10$ and $\Omega=100$, and we consider different detunings. The results may be understood from Eqs. (27)–(32). It is not difficult to see from Eqs. (29) and (30) that the inner sidebands $\Lambda_{1,2}$ will be very small, as $\rho_{bb}\simeq0$ and $\varepsilon^2\simeq0$. Hence the central line and the outer sidebands will dominate. This is evident in all the spectra of Fig. 5, but particularly for frame 5(a) where the inner sidebands are hardly visible. When the cavity frequency $\delta=0$, the spectrum is a symmetric, Mollow-like triplet, while the lower-frequency outer sideband is enhanced and the higher-frequency one suppressed when $\delta=\Omega_R$ and $2\Omega_R$. These features are similar to those of a laser-dressed two-level atom coupled to such a cavity field [7]. The enhancement and suppression of the sidebands is due to the cavity modification of the transition rates $|a\rangle\rightarrow|c\rangle$ and $|c\rangle\rightarrow|a\rangle$. The former decreases while the latter increases for $\delta=\Omega_R,2\Omega_R$. Therefore the enhanced spectral line of the outer sidebands is narrowed while the suppressed one is broadened. For large values of the detuning, shown in frame (d), the spectrum reverts to a symmetric form.

Next, we display the modified spectrum in the limit of $\omega_{21}\gg\Omega$ in Fig. 6 where the values $\omega_{21}=200$ and $\Omega=50$ are taken. Contrary to the spectra of Fig. 5, the inner sidebands are most pronounced for the $\delta=0$ situation, whereas the outer spectral lines are almost invisible. Tuning the cavity frequency may also change the spectral profile: the higher-frequency sideband is somewhat enhanced when $\delta=\Omega_R$ and $2\Omega_R$. As we discussed above, in the limit of $\omega_{21}\gg\Omega$, the dressed-state populations ρ_{aa} and ρ_{cc} are close to zero while $\rho_{bb}\simeq1$, and all the populations are barely dependent on the cavity frequency. It is obvious from Eqs. (29) and (30) that the $\Lambda_{1,2}$ are mainly determined by the cavity-frequency-dependent decay rates, Γ_{3a} and Γ_{3b}. For the parameters of Fig. 6, we have $\Gamma_{3a}(\delta=0)=\Gamma_{3a}(\delta=0)\simeq2.51$, $\Gamma_{3a}(\delta=\Omega_R)\simeq1.33$, $\Gamma_{3b}(\delta=\Omega_R)\simeq4.40$, and $\Gamma_{3a}(\delta=2\Omega_R)=0.93$, $\Gamma_{3b}(\delta=2\Omega_R)\simeq2.50$. Therefore $\Lambda_1(\omega=-\Omega_R)<\Lambda_2(\omega=\Omega_R)$, which implies that the lower-frequency peak is lower than the higher-frequency sideband.

In Fig. 7, we take the values $\omega_{21}=200$, $\Omega=100$, which correspond to the populations shown in frame (d) of Fig. 4. For $\delta=0$, the bulk of the population is concentrated in state $|b\rangle$, and there is little population in states $|a\rangle$ and $|c\rangle$. Hence the outer sidebands are weak in amplitude, while the inner sidebands and the central peak are pronounced. Tuning the laser to $\delta=\Omega_R$ or $\delta=2\Omega_R$ increases the relative amplitude of the high-frequency or low-frequency inner sideband, respectively. As δ is increased through $\delta=\Omega_R$ to $\delta=2\Omega_R$, the population in state $|a\rangle$ increases, while that in state $|c\rangle$ decreases. The low-frequency outer sideband consequently increases in amplitude at the expense of the amplitude of the high-frequency outer sideband.

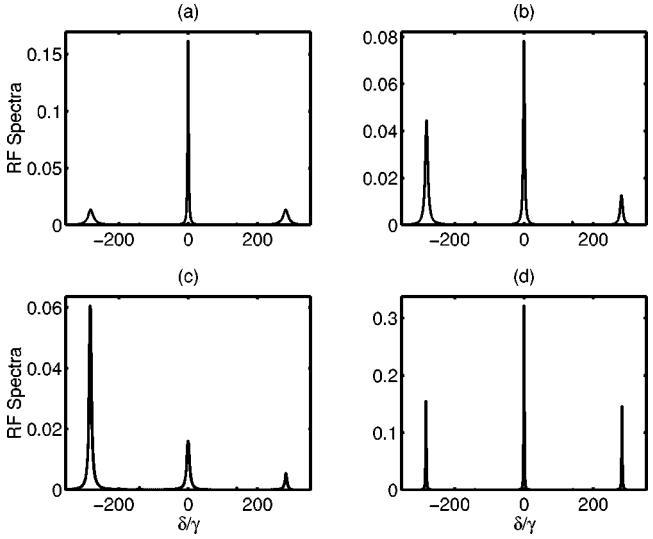

FIG. 5. The fluorescence spectrum for $\omega_{21}=10$, $\Omega=100$, and (a) $\delta=0$, (b) $\delta=\Omega_R$, (c) $\delta=2\Omega_R$, and (d) $\delta=10\Omega_R$, respectively.

For the general case, by inspection of Eqs. (26) for the cavity-induced decay rates Γ_i, one finds in the limit $\Omega_R \gg \kappa$ that, if the cavity is tuned to resonance with the driving laser ($\delta=0$), the rates are the same as those in free space [12], except for Γ_3 and Γ_5 being replaced by $\Gamma_3+\gamma_c 2\eta^2$ and $\Gamma_5+\gamma_c 8\eta^2$, respectively. This reflects the fact that the cavity-induced spontaneous emission rates can be greatly suppressed by increasing the Rabi frequency [7]. As shown in Fig. 8(a) for $\omega_{21}=200$ and $\Omega=200$, the inner and outer sidebands are broadened, while the central peak is narrowed.

We illustrate the spectra for $\delta=\Omega_R$ and $2\Omega_R$ in frames 8(b) and 8(c), respectively, where asymmetric spectral features are exhibited. The previous explanations apply to this case as well; that is, the enhancement and suppression of the spectral lines stems from the cavity modification of the dressed-state population distribution and decay rates. For example, for $\delta=2\Omega_R$ the population in the dressed state $|a\rangle$ is

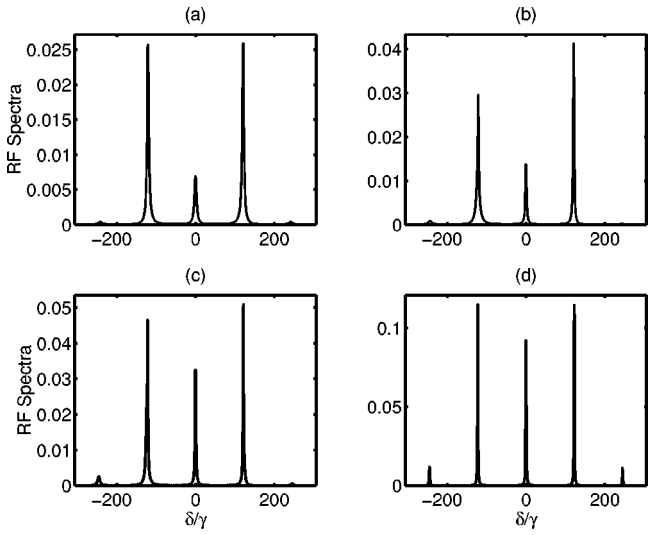

FIG. 6. The fluorescence spectrum for $\omega_{21}=20$, $\Omega=50$, and (a) $\delta=0$, (b) $\delta=\Omega_R$, (c) $\delta=2\Omega_R$, and (d) $\delta=10\Omega_R$, respectively.

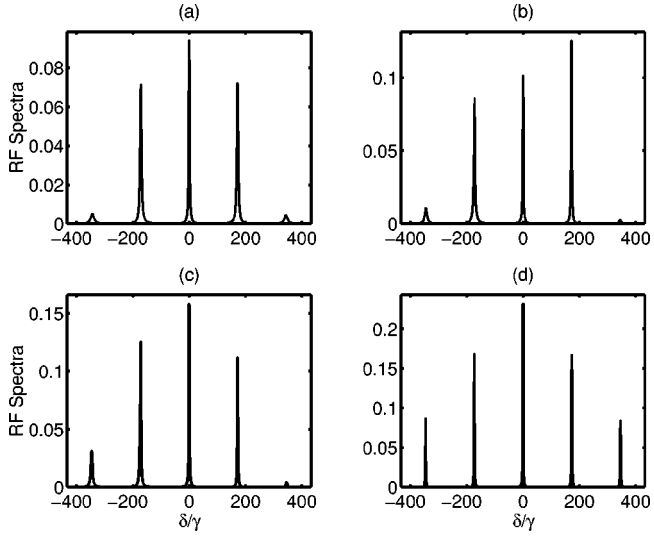

FIG. 7. The fluorescence spectrum for $\omega_{21}=200$, $\Omega=100$, and (a) $\delta=0$, (b) $\delta=\Omega_R$, (c) $\delta=2\Omega_R$, and (d) $\delta=10\Omega_R$, respectively.

much greater than those in the dressed states $|b\rangle$ and $|c\rangle$, as shown in Fig. 4(e). Accordingly, the lower-frequency peaks are higher than their counterparts in the high-frequency side.

V. ABSORPTION SPECTRUM

It is also natural to study the absorption spectrum of a weak, tunable probe field transmitted through the system, as we would expect this to be largely determined by the dressed-state populations. The frequency ω of the driving laser is kept fixed, and the absorption is measured as a function of the frequency ν of the probe laser, measured from the laser frequency ω. The absorption spectrum is given by

$$\mathcal{A}(\nu)=\mathrm{Re}\int_0^\infty \{\langle[A_{20}(t+\tau),A_{02}(t)]\rangle + \langle[A_{10}(t+\tau),A_{01}(t)]\rangle\}_{t\to\infty} e^{i\nu\tau} d\tau. \quad (33)$$

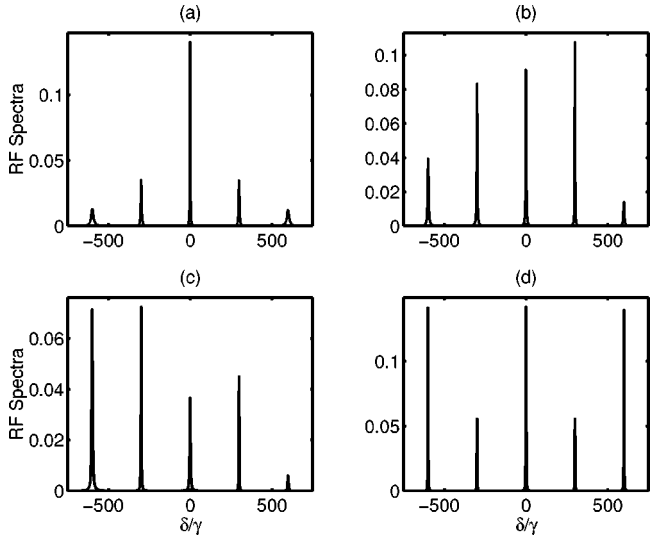

FIG. 8. The fluorescence spectrum for $\omega_{21}=200$, $\Omega=200$, and (a) $\delta=0$, (b) $\delta=\Omega_R$, (c) $\delta=2\Omega_R$ and (d) $\delta=10\Omega_R$, respectively.

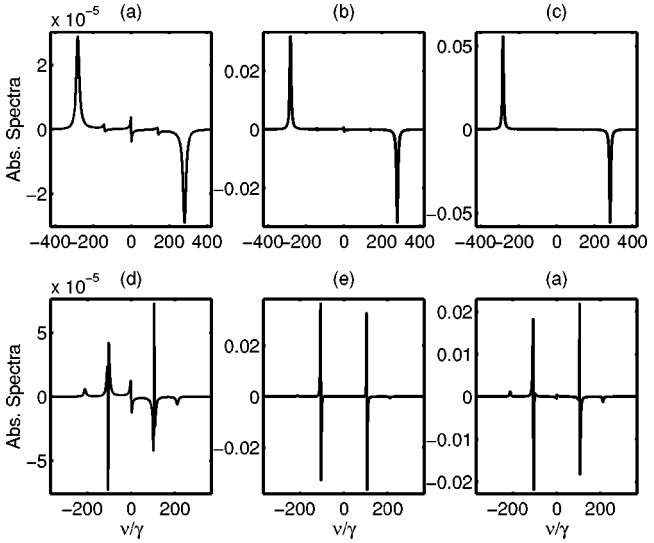

FIG. 9. The probe absorption spectrum. In the first three frames, $\omega_{21}=10$, $\Omega=100$, and in the last three $\omega_{21}=200$, $\Omega=50$. In frames (a) and (d), $\delta=0$, in frames (b) and (e), $\delta=\Omega_R$, and in frames (c) and (f), $\delta=2\Omega_R$, respectively.

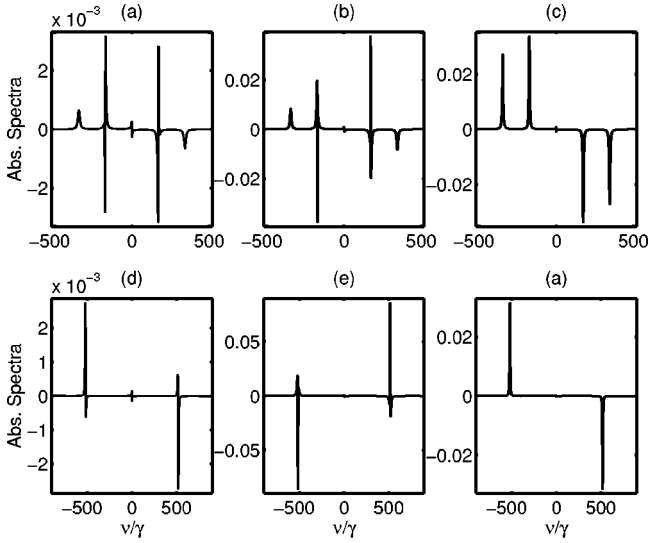

FIG. 10. The probe absorption spectrum. In the first three frames, $\omega_{21}=200$, $\Omega=100$, and in the last three $\omega_{21}=200$, $\Omega=200$. In frames (a) and (d), $\delta=0$, in frames (b) and (e), $\delta=\Omega_R$, and in frames (c) and (f), $\delta=2\Omega_R$, respectively.

We present only a brief discussion of this phenomenon here. As for the resonance fluorescence spectrum, we may use the quantum regression theorem to express the probe spectrum as

$$\mathcal{A}(\omega)=\mathrm{Re}[\tilde{F}_{01}(z)+\tilde{G}_{02}(z)-\tilde{F}'_{10}(z)-\tilde{G}'_{20}(z)]_{z=i\nu}, \tag{34}$$

where

$$F'(\tau)=U^{\dagger}(\tau)[\rho(\infty)|1\rangle\langle 0|]U(\tau)$$

and

$$G'(\tau)=U^{\dagger}(\tau)[\rho(\infty)|2\rangle\langle 0|]U(\tau). \tag{35}$$

It is possible to use the secular approximation to obtain expressions for the spectral components, as was done in the preceding section. However, for brevity, we concentrate on a qualitative discussion here.

In Fig. 9, frames (a)–(c) show the spectra for $\omega_{21}=10$, $\Omega=100$, ($\Omega_R=141.5$) when most of the population resides in the dressed states $|a\rangle$ and $|c\rangle$, and the population in state $|b\rangle$ is practically zero, although the latter does show a very small maximum for zero detuning, $\delta=0$. The case $\delta=0$ is shown in frame (a). Because there is no population in state $|b\rangle$, the absorption spectrum is largely determined by the transitions between the outer two levels from $|c\rangle$ to $|a\rangle$, at frequency $\nu\simeq 2\Omega_R$, and by the transitions between the inner two levels $|a\rangle$ to $|c\rangle$, at frequency $\nu\simeq -2\Omega_R$. For example, from Fig. 4, following the arguments of Cohen-Tannoudji and Reynaud [13], one can write down an approximate expression for the weight of the line at $\nu\simeq -2\Omega_R$ as

$$w_a(-2\Omega_R)\simeq P_aR_{ac}-P_cR_{ca}, \tag{36}$$

a negative value for w representing amplification, and a positive value absorption. It is easily seen that

$$w_a(+2\Omega_R)\simeq P_cR_{ca}-P_aR_{ac},=-w_a(-2\Omega_R). \tag{37}$$

Since the populations in levels $|a\rangle$ and $|c\rangle$ are equal when $\delta=0$, the difference between absorption and amplification is determined by the value of the rates.

A similar argument gives

$$\begin{aligned} w_a(-\Omega_R)&\simeq P_cR_{cb}+P_bR_{ba}-P_bR_{bc}-P_aR_{ab}\\ &\simeq P_cR_{cb}-P_aR_{ab}. \end{aligned} \tag{38}$$

Using the expressions from Eq. (18) for the rates, we find

$$\left|\frac{w_a(-\Omega_R)}{w_a(+2\Omega_R)}\right|\simeq\frac{\omega_{21}^2}{4\Omega_R^2}\ll 1. \tag{39}$$

These arguments explain the main features of the plot presented in frame (a). In frame (b), we tune the driving laser to $\delta=\Omega_R$, which has the effect of significantly increasing the population in $|c\rangle$ and decreasing that in level $|a\rangle$. The magnitudes of the absorption at $\nu\simeq -2\Omega_R$ and the emission at $\nu\simeq 2\Omega_R$ are thus greatly increased. The difference between the populations $|a\rangle$ and $|c\rangle$ reaches a maximum for $\delta=\pm 2\Omega_R$. This value of δ is assumed in frame (c), where the greatest absorption/emission occurs.

In frames (d)–(f), we change the parameters to $\omega_{21}=200$, $\Omega=50$ ($\Omega_R=122.5$). The populations for this case, whose behavior varies greatly from the preceding case, are shown in frame (c) of Fig. 4. Now we have a large population in state $|b\rangle$, and only small populations in states $|a\rangle$ and $|c\rangle$. The absorption spectra are thus quite different: the strongest features occur at $\nu=\pm\Omega_R$, and have a strong dispersive element, whereas the features at $\nu=\pm 2\Omega_R$ are relatively insignificant. Tuning the driving laser to $\delta=\pm\Omega_R$ or δ

$=\pm 2\Omega_R$ again has the effect of greatly increasing the strengths of the absorptions/emissions.

The first three frames of Fig. 10 show the absorption spectra for $\omega_{21}=200$, $\Omega=100$ ($\Omega_R=173.2$) and the second three frames the absorption spectra for $\omega_{21}=200$, $\Omega=200$ ($\Omega_R=300$). In these two cases, changing the detuning δ has a greater effect than in the cases of the preceding figure. This is particularly true in the last three frames, where it can be seen that changing the detuning can cause a switch from strong absorption to strong emission, and vice versa.

VI. CONCLUSIONS

We have investigated, in the bad-cavity limit, the resonance fluorescence of a V-type three-level atom strongly driven by a laser field and weakly coupled to a cavity mode, and we have demonstrated how the fluorescence may be controlled and manipulated by varying the cavity and Rabi frequencies. A strong dependency of the bare- and dressed-state populations on the cavity-resonant frequency is shown. Population inversion in both the bare- and dressed-state bases can be achieved for appropriate atom-cavity coupling constants, cavity-resonant frequency, and high-driving intensities. These population inversions result from the enhanced atom-cavity interaction when the cavity is tuned to resonance with the atomic dressed-state transition. The resultant fluorescence spectrum is also strongly dependent on the cavity frequency. When the cavity is resonant with the driving field, the spectrum is symmetric. Specifically, if the excited levels of the atom are degenerate (or near-degenerate), a Mollow-like triplet is exhibited with central line narrowing, but the spectrum has a two-peak structure if the level splitting is much greater than the laser intensity. Otherwise, the spectrum consists of five peaks. When the cavity is tuned to resonance with one of the spectral sidebands, some of the spectral lines may be enhanced and others suppressed, and so the spectrum is asymmetric. Dynamical line narrowing and peak suppression of certain spectral lines can be achieved by increasing the laser intensity. We have also demonstrated that a large degree of control and manipulation of the probe absorption spectrum can be achieved by tuning the cavity.

ACKNOWLEDGMENTS

J.S.P. wishes to thank the Royal Society London for financial support. This work is supported by the Natural Science Foundation of China and the United Kingdom EPSRC.

[1] See, for example,*Cavity Quantum Electrodynamics*, edited by P. R. Berman (Academic, London, 1994), and references therein.

[2] E. M. Purcell, Phys. Rev. **69**, 681 (1946); D. J. Heinzen and M. S. Feld, Phys. Rev. Lett. **59**, 2623 (1987).

[3] D. Kleppner, Phys. Rev. Lett. **47**, 233 (1982); D. J. Heinzen, J. J. Childs, J. E. Thomas, and M. S. Feld, *ibid.* **58**, 1320 (1987).

[4] C. Cohen-Tannoudji and S. Reynaud, J. Phys. B **10**, 345 (1977).

[5] J.-S. Peng and G.-X. Li, *Introduction to Modern Quantum Optics* (World Scientific, Singapore, 1998).

[6] M. Lewenstein, T. W. Mossberg, and R. J. Glauber, Phys. Rev. Lett. **59**, 775 (1987); M. Lewenstein and T. W. Mossberg, Phys. Rev. A **37**, 2048 (1988).

[7] P. Zhou and S. Swain, Phys. Rev. A **58**, 1515 (1998); **57**, 3871 (1997).

[8] H. Freedhoff and T. Quang, Phys. Rev. Lett. **72**, 474 (1994); J. Opt. Soc. Am. B **10**, 1337 (1994); **12**, 9 (1995).

[9] M. Loffler, G. M. Meyer, and H. Walther, Phys. Rev. A **55**, 3923 (1997).

[10] W. Lange and H. Walther, Phys. Rev. A **48**, 4551 (1993); G. S. Agarwal, W. Lange, and H. Walther, *ibid.* **48**, 4555 (1993).

[11] Y. Zhu, A. Lezama, T. W. Mossberg, and M. Lewenstein, Phys. Rev. Lett. **61**, 1946 (1988); A. Lezama, Y. Zhu, S. Morin, and T. W. Mossberg, Phys. Rev. A **39**, R2754 (1989).

[12] P. Zhou and S. Swain, Phys. Rev. Lett. **77**, 3995 (1996); Phys. Rev. A **56**, 3011 (1997).

[13] C. Cohen-Tannoudji and S. Reynaud, in *Multiphoton Processes*, edited by J. H. Eberly and P. Lambropoulos (Wiley, New York, 1978), p. 103.